POISSON-NERNST-PLANCK SYSTEMS FOR ION FLOW WITH DENSITY FUNCTIONAL THEORY FOR HARD-SPHERE POTENTIAL: I-V RELATIONS AND CRITICAL POTENTIALS. PART II: NUMERICS

WEISHI LIU*, XUEMIN TU†, AND MINGJI ZHANG‡

Abstract. We consider a one-dimensional steady-state Poisson-Nernst-Planck type model for ionic flow through membrane channels. Improving the classical Poisson-Nernst-Planck models where ion species are treated as point charges, this model includes ionic interaction due to finite sizes of ion species modeled by hard sphere potential from the Density Functional Theory. The resulting problem is a singularly perturbed boundary value problem of an integro-differential system. We examine the problem and investigate the ion size effect on the current-voltage (I-V) relations numerically, focusing on the case where two oppositely charged ion species are involved and only the hard sphere components of the excess chemical potentials are included. Two numerical tasks are conducted. The first one is a numerical approach of solving the boundary value problem and obtaining I-V curves. This is accomplished through a numerical implementation of the analytical strategy introduced by Ji and Liu in [*Poisson-Nernst-Planck systems for ion flow with density functional theory for hard-sphere potential: I-V relations and critical potentials. Part I: Analysis, submitted*]. The second task is to numerically detect two critical potential values V_c and V^c. The existence of these two critical values is first realized for a relatively simple setting and analytical approximations of V_c and V^c are obtained in the above mentioned reference. We propose an algorithm for numerical detection of V_c and V^c *without using any analytical formulas* but based on the defining properties and numerical I-V curves directly. For the setting in the above mentioned reference, our numerical values for V_c and V^c agree well with the analytical predictions. For a setting including a nonzero permanent charge in which case no analytic formula for the I-V relation is available now, our algorithms can still be applied to find V_c and V^c numerically.

Key words. Ion flow, PNP-DFT, hard-sphere, I-V relation, critical potentials

AMS subject classifications. 34D15, 45J05, 65L10, 78A35, 92C35

1. Introduction.

We numerically examine singularly perturbed boundary value problems of an integro-differential system – a one-dimensional steady-state Poisson-Nernst-Planck (PNP) type model for ionic flow through membrane channels. Fundamental models for electrodiffusion process of charged particles are the Langevin-Poisson system at the molecular scale (see, for example, [2, 7, 8, 12, 37, 47, 49, 56, 57, 61]) and the Maxwell-Boltzmann equation for continuum versions (see, for example, [4, 36, 37, 56, 66]). Analysis as well as numerics on these models are very challenging. PNP type systems are a well-accepted class of reduced models in a wide range of physical problems of biological units ([3, 9, 11, 14, 27, 28, 29, 36, 37, 56, 57], etc.). They can be derived from the Langevin systems and the Maxwell-Boltzmann equation (see [4, 61]) and from the energetic variational analysis *EnVarA* (see [16, 17, 34, 35]).

The simplest PNP type model is the classical Poisson-Nernst-Planck (cPNP) systems for which only the ideal component of the electrochemical potential is included. To a great extent, the cPNP system has been simulated (see, e.g., [9, 10, 11, 13, 15, 29, 31, 32, 33, 37, 42, 48, 60]) and analyzed (see, e.g., [1, 5, 6, 18, 22, 43, 44, 45, 50, 58, 59, 62, 63, 64, 65]). The basic assumption in the derivation of cPNP systems is a "dilute" assumption so that one can treat ions as point-charges. In particular, cPNP systems treat ions with the equal valences essentially the same except it associates different diffusion coefficients to ions species with different ion sizes. Clearly, this over-simplification of cPNP systems could be a serious defect for modeling in many biological situations; for example, both Na (sodium) and K (potassium)

---

*Department of Mathematics, University of Kansas,1460 Jayhawk Blvd., Room 405, Lawrence, Kansas 66045 (`wliu@math.ku.edu`). This author's work was supported in part by National Science Foundation contract DMS-0807327.

†Department of Mathematics, University of Kansas, 1460 Jayhawk Blvd., Room 405, Lawrence, Kansas 66045 (`xtu@math.ku.edu`). This author's work was supported in part by National Science Foundation contract DMS-1115759.

‡Department of Mathematics, University of Kansas,1460 Jayhawk Blvd., Room 405, Lawrence, Kansas 66045 (`mingjizhang@math.ku.edu`). This author's work was supported in part by National Science Foundation contract DMS-0807327.

ions have the same valence (+1) but they have significantly different biological properties due mainly to their different sizes. [1]

To take into considerations of ion sizes, one needs to include the excess (beyond the ideal) chemical potential in the model. The PNP system combined with Density Functional Theory (DFT) for hard sphere potentials of ion species serves the purpose for this consideration and has been investigated computationally with great improvements ([23, 24, 25, 26, 29, 39, 41], etc.). All these computations, however, lack sufficiently analytical supports. In a recent work [38], the authors analyzed a one-dimensional version of PNP-DFT system in a simple setting; they considered the case where two oppositely charged ions are involved, the permanent charge can be ignored and only the hard sphere component of the excess chemical potential is included beyond the ideal potential. The model, viewed as a singularly perturbed boundary value problem of an integro-differential system, was analyzed by a combination of geometric singular perturbation theory and functional analysis. They established the existence result for small ion sizes and, treating the sizes as small parameters, derived an approximation of the current-voltage (I-V) relation. The approximation result allowed them to make the following finding: there is a critical potential value V_c so that, if $V > V_c$, then the ion size enhances the current; if $V < V_c$, it reduces the current; There is another critical potential value V^c so that, if $V > V^c$, the current is increasing with respect to $\lambda = r_2/r_1$ where r_1 and r_2 are, respectively, the radii of the positively and negatively charged ions; if $V < V^c$, the current is decreasing in λ.

In this paper, we perform numerical study of the one-dimensional version of PNP-DFT system in a more general setting than that in [38] to include non-trivial permanent charges. Two numerical tasks are conducted. The first one is a numerical approach for solving the boundary value problem and obtaining I-V curves. This is accomplished through a numerical implementation of the analytical strategy introduced in [38]. The second task is to numerically detect two critical potential values V_c and V^c that are defined slightly general than those in [38]. Without analytical formulas for general situations, we propose an algorithm for numerical detection of V_c and V^c *without using any analytical formulas* but based on the defining properties and numerical I-V curves directly. For the setting used in [38], we apply our algorithm to obtain numerical values for V_c and V^c and the values agree well with the analytical predictions. For a setting including a nonzero permanent charge in which case no analytic formula for the I-V relation is available now, we can still apply the algorithm and find V_c and V^c numerically.

We remark that our numerical study in this paper is oriented by the two tasks described above. The numerical aspect is nontrivial due to the singular and nonlocal natures of the boundary value problem. On the other hand, it is not as challenging as it could be for the following reasons:

1. We are working on a *one-dimensional* version PNP-DFT model that is much simpler than a three-dimensional one. The excess chemical potential considered here only includes the hard sphere component.
2. For the setting in [38] without permanent charges, the analytical strategy reduces the boundary value problem to a fixed point problem and the corresponding mapping is a *contraction mapping* for small ion sizes. For this case, we are able to implement the analytical strategy to reduce our numerical problem to a numerical fixed point iteration. Also, the analytical zeroth order approximation of the true solution helps for a choice of a good initial guess for our numerical iteration.

The rest of the paper is organized as follows. In Section 2, we briefly set up the one-dimensional PNP-DFT model for ionic flows and recall the analytic results from [38]. In Section 3, we discuss our numerical strategy for solving the model problem in detail. In Section 4, we introduce two critical potentials generalizing those defined in [38] and propose an algorithm for numerical detections of the critical potentials. In Section 5, we present a

---

[1] Strictly speaking, the cPNP system does not completely ignore ion sizes in the sense that it involves diffusion coefficients of each individual ions species that do depend on ion sizes.

number of case studies to demonstrate the application of our algorithm. A conclusion remark is given in Section 6.

2. Models and two critical potentials.

In this section, we briefly recall the model of Poisson-Nernst-Planck (PNP) systems with hard sphere (HS) potentials for ion sizes and the main result in [38] on ion size effects to I-V relations.

The one-dimensional steady-state PNP type model for ionic flow is

$$\begin{aligned} &-\frac{1}{h(x)}\frac{d}{dx}\left(\varepsilon_r(x)\varepsilon_0 h(x)\frac{d\phi}{dx}\right) = e\left(\sum_{j=1}^{n} z_j c_j(x) + Q(x)\right), \\ &-J_i = \frac{1}{kT}D_i(x)h(x)c_i(x)\frac{d\mu_i}{dx}, \quad \frac{dJ_i}{dx} = 0, \quad i = 1, 2, \cdots, n \end{aligned} \tag{2.1}$$

on $x \in (0,1)$ with the boundary conditions

$$\phi(0) = V,\ c_i(0) = L_i; \quad \phi(1) = 0,\ c_i(1) = R_i, \tag{2.2}$$

where e is the elementary charge, k the Boltzmann constant, T the absolute temperature; ϕ is the electric potential, $Q(x)$ the permanent charge of the channel, $\varepsilon_r(x)$ the dielectric constant (relative permittivity), ε_0 the vacuum permittivity, n the number of distinct ion species; for the ith ion species, c_i is the concentration, z_i the valence (the number of charges per particle), μ_i the electrochemical potential, J_i the flux density, and $D_i(x)$ the diffusion coefficient; $h(x)$ represents the cross-section area of the channel over the point x. For more details, see, for example, [29, 38, 48].

Through out the paper, we will assume the electroneutrality conditions at the boundaries

$$\sum_{j=1}^{n} z_j L_j = \sum_{j=1}^{n} z_j R_j = 0. \tag{2.3}$$

For fixed L_i's and R_i's, a solution (ϕ, c_i, J_i) of (2.1) and (2.2) depends on V and the so-called I-V (current-voltage) relation is

$$I(V) = \sum_{j=1}^{n} z_j e J_j(V; L_i, R_i). \tag{2.4}$$

The electrochemical potential μ_i for the ith ion species consists of the concentration-independent component $\mu_i^0(x)$ (e.g. a hard-well potential), the ideal component $\mu_i^{id}(x)$, and the excess component $\mu_i^{ex}(x)$:

$$\mu_i(x) = \mu_i^0(x) + \mu_i^{id}(x) + \mu_i^{ex}(x)$$

where

$$\mu_i^{id}(x) = z_i e\phi(x) + kT\ln\frac{c_i(x)}{c_0} \tag{2.5}$$

with some characteristic number density c_0. The excess chemical potential $\mu_i^{ex}(x)$ to account for the finite size effect of charges consists of two components: the hard-sphere component μ_i^{HS} and the electrostatic component μ_i^{ES}([54, 55]); that is,

$$\mu_i^{ex} = \mu_i^{HS} + \mu_i^{ES}.$$

The Density Functional Theory (DFT) ([19, 20], etc.) states that $\mu_i^{ex}(x)$ is actually a functional of the *concentrations*, $\{c_j(x)\}$. But no exact formula for the functional dependence is available in general.

For one-dimensional hard-sphere potential μ_i^{HS} with two ion species, one has ([21, 51, 52, 53, 54, 55])

$$\mu_i^{HS} = kT\frac{\delta\Omega(\{c_j\})}{\delta c_i}, \tag{2.6}$$

where

$$\begin{aligned}\Omega(\{c_j\}) &= -\int n_0(x;c_1,c_2)\ln(1-n_1(x;c_1,c_2))dx,\\ n_l(x;c_1,c_2) &= \sum_{j=1}^{2}\int c_j(x')\omega_l^j(x-x')dx', \quad (l=0,1),\\ \omega_0^j(x) &= \frac{\delta(x-r_j)+\delta(x+r_j)}{2}, \quad \omega_1^j(x) = \Theta(r_j-|x|),\end{aligned} \tag{2.7}$$

where δ is the Dirac delta function, Θ is the Heaviside function with $\Theta(x)=0$ for $x<0$ and $\Theta(x)=1$ for $x\geq 0$, and r_j is the radius of the jth ion species.

In [38], the authors considered only the hard-sphere component μ_i^{HS} of μ_i^{ex} with two ion species ($n=2$) of opposite charges ($z_1>0$ and $z_2<0$) and $Q=0$. The authors assumed that $\varepsilon_r(x)=\varepsilon_r$ and $D_j(x)=D_j$'s are constants. Based on a combination of geometric singular perturbation analysis and functional analysis, the existence and uniqueness result for the boundary value problem (BVP) (2.1)–(2.2) is established. Assuming further that $h(x)=1$, an approximation of I-V relation in $r=r_1$ is also obtained:

$$I(V;\varepsilon,r) := z_1eJ_1+z_2eJ_2 = I_0(V;\varepsilon)+I_1(V;\varepsilon)r+o(r),$$

where

$$\varepsilon^2 = \frac{\varepsilon_r\varepsilon_0 kT}{e^2},$$

and

$$\begin{aligned}I_0(V;0) &= e(D_1-D_2)(L-R)+\frac{e^2(z_1D_1-z_2D_2)}{kT}f_0(L,R)V,\\ I_1(V;0) &= \frac{2e(L-R)}{z_1z_2}[(\lambda-1)(z_1D_1-z_2D_2)f_0(L,R)-(z_1\lambda-z_2)(D_1-D_2)(L+R)]\\ &\quad -\frac{2e^2(z_1\lambda-z_2)(z_1D_1-z_2D_2)}{z_1z_2kT}f_1(L,R)V,\end{aligned}$$

with $\lambda=r_2/r_1$, $L=z_1L_1=-z_2L_2>0$, $R=z_1R_1=-z_2R_2>0$,

$$f_0(L,R) = \frac{L-R}{\ln L-\ln R}, \quad f_1(L,R) = \frac{(L^2-R^2)(\ln L-\ln R)-2(L-R)^2}{(\ln L-\ln R)^2}.$$

This explicit approximation allows the authors of [38] to realize the existence of two critical potential values V_c and V^c defined, respectively, by

$$I_1(V_c;0)=0, \quad \frac{d}{d\lambda}I_1(V^c;0)=0. \tag{2.8}$$

They are given, in this setting, by

$$\begin{aligned}V_c &= \frac{kT}{e}\left((\lambda-1)\frac{(L-R)f_0(L,R)}{(z_1\lambda-z_2)f_1(L,R)}-\frac{(D_1-D_2)(L^2-R^2)}{(z_1D_1-z_2D_2)f_1(L,R)}\right),\\ V^c &= \frac{kT}{e}\left(\frac{(L-R)f_0(L,R)}{z_1f_1(L,R)}-\frac{(D_1-D_2)(L^2-R^2)}{(z_1D_1-z_2D_2)f_1(L,R)}\right).\end{aligned} \tag{2.9}$$

The importance of V_c and V^c is evident and we summarize the result from [38] here.

THEOREM 2.1. *Let V_c and V^c be defined by (2.8).*

(i) *If $V > V_c$, then for $\varepsilon > 0$ small and $r > 0$ small, the ion sizes enhance the current I; that is, $I(V;\varepsilon,r) > I(V;\varepsilon,0)$;*
If $V < V_c$, then for $\varepsilon > 0$ small and $r > 0$ small, the ion sizes reduce the current I; that is, $I(V;\varepsilon,r) < I(V;\varepsilon,0)$;

(ii) *If $V > V^c$, then for $\varepsilon > 0$ small and $r > 0$ small, the larger the negatively charged ion the larger the current I; that is, the current I is increasing in λ;*
If $V < V^c$, then for $\varepsilon > 0$ small and $r > 0$ small, the smaller the negatively charged ion the larger the current I; that is, the current I is decreasing in λ.

3. Numerical solution of the BVP (2.1)–(2.2). Motivated by the work in [38] and with a longterm goal of understanding effects of various parameters (such as ion sizes, permanent charges, boundary conditions, etc.) on I-V relations of membrane channels, we examine the effect of ion sizes on the I-V relation based on numerical solutions of the BVP (2.1)–(2.2). We will conduct two numerical tasks.

Task 1. We will develop a numerical approach to obtain the numerical solution of the BVP (2.1)–(2.2) and, as a result, obtain numerical I-V curves.

Task 2. Based on numerical I-V curves and the defining properties of V_c and V^c (NOT the analytical formulas (2.9)), we will propose an algorithm for detecting V_c and V^c numerically and test the algorithm for two cases:

(a) for $Q = 0$ that allows us to make a comparison between the analytical predications in [38] and our numerical results;
(b) for a piece-wise constant $Q \neq 0$ where no analytical formulas for V_c and V^c are currently available.

In this section, we will carry out the first task. Task 2 is a critical component for the relevance of our mathematical studies of the PNP type models to ion channel properties and will be carried out in Section 4.

To this end, we recall the dimensionless form of (2.1)–(2.2) made in [38]. Assume the relative permittivity $\varepsilon_r(x) = \varepsilon_r$ and the diffusion coefficient $D_i(x) = D_i$ are constants and $h(x) = 1$. Substituting the expression (2.5) for $\mu_i^{id}(x)$, the expression (2.6) for $\mu_i^{HS}(x)$, and making the dimensionless re-scaling,

$$\bar{\phi} = \frac{e}{kT}\phi, \quad \bar{V} = \frac{e}{kT}V, \quad \varepsilon^2 = \frac{\varepsilon_r\varepsilon_0 kT}{e^2}, \quad \bar{J}_i = \frac{J_i}{D_i}, \tag{3.1}$$

we get the following one-dimensional steady-state PNP-DFT system for two ion species with valences $\alpha = z_1 > 0$ and $-\beta = z_2 < 0$:

$$\begin{aligned}
&\varepsilon^2\frac{d^2\bar{\phi}}{dx^2} = -(\alpha c_1 - \beta c_2 + Q(x)), \quad \frac{d\bar{J}_i}{dx} = 0,\\
&\frac{dc_1}{dx} + \alpha c_1\frac{d\bar{\phi}}{dx} + \frac{c_1(x)}{kT}\frac{d}{dx}\mu_1^{HS}(x) = -\bar{J}_1,\\
&\frac{dc_2}{dx} - \beta c_2\frac{d\bar{\phi}}{dx} + \frac{c_2(x)}{kT}\frac{d}{dx}\mu_2^{HS}(x) = -\bar{J}_2.
\end{aligned} \tag{3.2}$$

The boundary conditions are

$$\bar{\phi}(0) = \bar{V}, \quad c_i(0) = L_i; \quad \bar{\phi}(1) = 0, \quad c_i(1) = R_i. \tag{3.3}$$

The following technical result (Lemma 4.2 in [38]) will be used in our numerical simulation. For $x \in [0,1]$,

$$\begin{aligned}
\frac{1}{kT}\frac{d\mu_1^{HS}}{dx}(x) =& \frac{c_1(x+2r) + c_2(x+(\lambda+1)r)}{1-K_1(x)} - \frac{c_1(x-2r) + c_2(x-(\lambda+1)r)}{1-K_2(x)},\\
\frac{1}{kT}\frac{d\mu_2^{HS}}{dx}(x) =& \frac{c_1(x+(\lambda+1)r) + c_2(x+2\lambda r)}{1-K_3(x)} - \frac{c_1(x-(\lambda+1)r) + c_2(x-2\lambda r)}{1-K_4(x)},
\end{aligned} \tag{3.4}$$

where

$$\begin{aligned} K_1(x) &= \int_x^{x+2r} c_1(s)ds + \int_{x-(\lambda-1)r}^{x+(\lambda+1)r} c_2(s)ds, \\ K_2(x) &= \int_{x-2r}^{x} c_1(s)ds + \int_{x-(\lambda+1)r}^{x+(\lambda-1)r} c_2(s)ds, \\ K_3(x) &= \int_{x+(\lambda-1)r}^{x+(\lambda+1)r} c_1(s)ds + \int_{x}^{x+2\lambda r} c_2(s)ds, \\ K_4(x) &= \int_{x-(\lambda+1)r}^{x-(\lambda-1)r} c_1(s)ds + \int_{x-2\lambda r}^{x} c_2(s)ds. \end{aligned} \tag{3.5}$$

Remark 3.1. *The definition of $\mu_i^{HS}(x)$ for $x \in [0,1]$ requires (c_1, c_2) to be defined for $x \in [-\rho, 1+\rho]$ where $\rho = \max\{r_1 + r_2, 2r_1, 2r_2\}$. (Recall that r_1 and r_2 are the radii of the positively and negatively charged ions respectively.) As remarked in [38], the difference between the effects of different extensions is of order $O(\rho^2)$. In the sequel, we will fix an extension for our numerical simulations.*

3.1. Numerical strategy for solving problem (3.2)–(3.3). In this part, we present our numerical strategy for *Task 1.* Note that system (3.2) is an integro-differential system. Our numerical approach is to implement the analytical strategy in [38] that is one of the natural approaches to integro-differential systems.

We begin with a brief summary of the analytical strategy in [38]. For any $(G_1(x), G_2(x)) \in \mathcal{C}^0([0,1], \mathbb{R}^2)$, introduce the auxiliary problem

$$\begin{aligned} &\varepsilon^2 \frac{d^2\bar\phi}{dx^2} = -(\alpha c_1 - \beta c_2 + Q(x)), \quad \frac{d\bar J_i}{dx} = 0, \\ &\frac{dc_1}{dx} + \alpha c_1 \frac{d\bar\phi}{dx} + G_1(x) = -\bar J_1, \\ &\frac{dc_2}{dx} - \beta c_2 \frac{d\bar\phi}{dx} + G_2(x) = -\bar J_2 \end{aligned} \tag{3.6}$$

with the same boundary conditions in (3.3)

$$\bar\phi(0) = \bar V, \quad c_i(0) = L_i; \quad \bar\phi(1) = 0, \quad c_i(1) = R_i. \tag{3.7}$$

Let $\big(\bar\phi(x;\varepsilon), c_i(x;\varepsilon)\big)$ be the solution of (3.6) and (3.7) and define a mapping

$$\mathcal{F} : \mathcal{C}^0([0,1], \mathbb{R}^2) \to \mathcal{C}^1([0,1], \mathbb{R}^2) \text{ by } \mathcal{F}(G_1, G_2)(x) = (c_1(x;\varepsilon), c_2(x;\varepsilon)).$$

Define the second mapping

$$\mathcal{G} : \mathcal{C}^1([0,1], \mathbb{R}^2) \to \mathcal{C}^0([0,1], \mathbb{R}^2)$$

by

$$\mathcal{G}(c_1, c_2)(x) = \left(\frac{c_1(x)}{kT} \frac{d}{dx} \mu_1^{HS}(x), \frac{c_2(x)}{kT} \frac{d}{dx} \mu_2^{HS}(x) \right),$$

where μ_i^{HS} are given by the model (2.6) for the given (c_1, c_2).

The BVP (3.2) and (3.3) becomes a fixed point problem

$$(G_1, G_2) = \mathcal{H}(G_1, G_2) \text{ for } (G_1, G_2) \in \mathcal{C}^0([0,1], \mathbb{R}^2) \tag{3.8}$$

where $\mathcal{H} = (\mathcal{G} \circ \mathcal{F})$. It has been proved in [38, Theorem 5.1] that, for $\varepsilon > 0$ small and as $r \to 0$, the Fréchet derivative $D\mathcal{H}$ of $\mathcal{H}$ is of order $O(r)$. Hence, for $\varepsilon > 0$ small and r small, $\mathcal{H}$ is a contraction mapping and it has a unique fixed point.

Our numerical approach, in a simple word, is to solve the above fixed point problem by numerical iterations. Since the mapping $\mathcal{H}$ is not explicit, a numerical approximation $\mathcal{H}_N$ of $\mathcal{H}$ cannot be directly constructed. Instead, we will numerically implement the above analytical strategy, that is, we proceed to construct numerical approximations of $\mathcal{F}$ and $\mathcal{G}$ with two subroutines. We now describe the iteration procedure.

Subroutine 1. Given fixed functions $G_1^{(0)}(x)$ and $G_2^{(0)}(x)$, we numerically solve the BVP (3.6) and (3.7) with $G_i(x) = G_i^{(0)}(x)$. This auxiliary problem is a BVP of ordinary differential equations (ODEs). We could use standard BVP solvers for ODEs to obtain the numerical solutions $\big(\bar\phi^{(0)}, u^{(0)}, c_1^{(0)}, c_2^{(0)}, \bar J_1^{(0)}, \bar J_2^{(0)}\big)$ for $x \in [0,1]$.

Subroutine 2. After an extension of $(c_1^{(0)}, c_2^{(0)})$ to $x \in [-\rho, \rho+1]$, we numerically determine $\big(G_1^{(1)}(x), G_2^{(1)}(x)\big)$ from

$$G_i^{(1)}(x) = \frac{c_i^{(0)}(x)}{kT}\frac{d}{dx}\mu_i^{HS}(x)$$

using (3.4) with $c_i(x) = c_i^{(0)}(x)$. This completes one numerical iteration:

$$\left(G_1^{(1)}, G_2^{(1)}\right) = \mathcal{H}_N\left(G_1^{(0)}, G_2^{(0)}\right). \tag{3.9}$$

The mapping $\mathcal{H}_N$ can be viewed as a numerical realization of $\mathcal{H} = \mathcal{G}\circ\mathcal{F}$. Our numerical fixed point iteration method can be formulated as

$$\left(G_1^{(n+1)}, G_2^{(n+1)}\right) = \mathcal{H}_N\left(G_1^{(n)}, G_2^{(n)}\right). \tag{3.10}$$

Subroutine 2 is straightforward because of the explicit formula (3.4). The convergence of this numerical fixed point iteration depends on BVP solvers for (3.6)–(3.7) involved in Subroutine 1. In our BVP solvers, we obtain our numerical solutions with the max norm of the absolute difference between two consecutive iterations less than 10^{-6}. With this requirement, the approximate solutions of our BVPs are close enough to the true solution such that the fixed point problem converges reasonably fast. See Section 3.2 for more details about our BVP solvers. Our numerical experiments reported in Section 5 show that, with the BVP solvers and the initial guess we used, the iterations (3.10) converge quite fast (usually need less than 5 iterations to reduce the L_2-error to 10^{-6}).

Before we discuss our BVP solvers and the initial guess in more detail below, we would like to briefly compare our work to the one in [41]. The model considered in our present paper is one dimensional and only hard sphere component of the excess chemical potential is included. Much more complicated three dimensional model is considered in [41] and their excess potential includes both the hard sphere and electrostatic components. Although both works uses iteration methods, the problem treated in [41] and the numerical task are much more challenging. We also take the advantage of the analysis in ([38]) in each iteration; more precisely, we calculate the hard sphere potential for (G_1, G_2) from formula (3.4) directly instead of (2.6) and (2.7) using the density functions (c_1 and c_2) from previous iteration, and $(\bar\phi, c_1, c_2)$ are then updated together with the BVP solvers for (3.6)–(3.7). For the one dimensional case we consider here, our fixed point iteration converges exponentially if the numerical solutions of the BVP system are accurate enough and r_1 and r_2 are small enough, see [38].

3.2. BVP solvers for (3.6)–(3.7) and the initial guess. We use "bvp4c" in Matlab ([40]) as the solver for our auxiliary BVP (3.6) and (3.7). It solves first order systems of ordinary differential equations with two-point boundary conditions of this form:

$$\begin{cases} y' = f(x,y), & a < x < b, \\ g(y(a), y(b)) = 0. \end{cases} \tag{3.11}$$

Given a mesh partition $a = x_0 < x_1 < \cdots < x_N = b$, the numerical solution of (3.11) is approximated by a piecewise cubic polynomial function $S(x)$. The approximated solution $S(x)$ satisfies the boundary conditions and it is a cubic Hermite interpolation polynomial for each subinterval $[x_i, x_{i+1}]$.

For $i = 0, 1, 2, \cdots, N-1$, let $y_i = S(x_i)$ and let $h_i = x_{i+1} - x_i$. The y_i's are evaluated by solving the algebraic equations

$$\Phi(X,Y) = (\phi_0(X,Y), \phi_1(X,Y), \cdots, \phi_N(X,Y)) = 0, \tag{3.12}$$

where

$$\begin{array}{rcl} X & = & [x_0, x_1, \cdots, x_N]^T, \\ Y & = & [y_0, y_1, \cdots, y_N]^T, \\ \phi_0(X,Y) & = & g(y_0, y_N), \\ \phi_i(X,Y) & = & y_i - y_{i-1} - \frac{1}{6}h_{i-1}(f_{i-1} + 4f_i^* + f_i), \quad i = 1, 2, \cdots, N, \end{array}$$

and

$$\begin{array}{rcl} f_i & = & f(x_i, y_i), \\ f_i^* & = & f\left(\frac{1}{2}(x_{i-1} + x_i), \frac{1}{2}(y_{i-1} + y_i) - \frac{1}{8}h_{i-1}(f_i - f_{i-1})\right). \end{array}$$

The algebraic system (3.12) is solved by simplified Newton's method with a weak line search. The global Jacobian $\frac{\partial \Phi}{\partial Y}$ (using finite difference approximation by default) is required and the structure of the Jacobian is important for the linear solver in each Newton's iteration. The residual of $S(x)$ is calculated by $r(x) = S(x) - f(x, S(x))$ and the residual in the boundary conditions is $g(S(a), S(b))$. The adaptive mesh strategy has been used to control the residual in "bvp4c", for details, see [40].

Due to the piecewise cubic approximate solution $S(x)$ given by "bvp4c", we could obtain the K_i's in (3.5) analytically and evaluate $G_1^{(n)}(x)$ and $G_2^{(n)}(x)$ accurately in each fixed point iteration. Moreover, we could extend the solution to $[-\rho, 1+\rho]$ easily for polynomials. In our numerical experiments, we use a constant extension.

To apply "bvp4c", we first rewrite (3.6) into a system of 1st-order equations as

$$\begin{aligned} &\varepsilon \frac{d\bar{\phi}}{dx} = \bar{u}, \\ &\varepsilon \frac{d\bar{u}}{dx} = -(\alpha c_1 - \beta c_2 + Q(x)), \quad \frac{d\bar{J}_i}{dx} = 0, \\ &\varepsilon \frac{dc_1}{dx} + \alpha c_1 \bar{u} + \varepsilon G_1(x) = -\varepsilon \bar{J}_1, \\ &\varepsilon \frac{dc_2}{dx} - \beta c_2 \bar{u} + \varepsilon G_2(x) = -\varepsilon \bar{J}_2 \end{aligned} \tag{3.13}$$

with the same boundary conditions in (3.6).

For a general iteration step, we take the initial guess from the approximate solution of the previous fixed point iteration. At the first iteration, for the case where $Q = 0$, we take advantage of the analysis from [38] and choose the initial guess $\left(\bar{\phi}^{(0,0)}, u^{(0,0)}, c_1^{(0,0)}, c_2^{(0,0)}, \bar{J}_1^{(0,0)}, \bar{J}_2^{(0,0)}\right)$ as follows.

The leading term for the analytical solution (G_1, G_2) is provided in [38, Theorem 6.1]. We take it as our initial guess

$$G_1^{(0)}(x) = n_1(L - (L-R)x), \quad G_2^{(0)}(x) = n_2(L - (L-R)x), \tag{3.14}$$

where

$$n_1 = -\frac{2(\alpha(\lambda+1) + 2\beta)(L-R)r}{\alpha^2 \beta kT}, \quad n_2 = -\frac{2(2\alpha\lambda + \beta(\lambda+1))(L-R)r}{\alpha \beta^2 kT}.$$

The leading terms for c_1 and c_2 are also provided in [38, Proposition 3.4] as

$$c_1^{(0,0)}(x) =\frac{L-(L-R)x+mx(1-x)}{\alpha}, \quad c_2^{(0,0)}(x) = \frac{L-(L-R)x+mx(1-x)}{\beta},$$

where

$$m = \frac{2(\alpha\lambda+\beta)(L-R)^2}{\alpha\beta kT}r.$$

Using the expressions for $\bar{J}_1^{(0,0)}$, $\bar{J}_2^{(0,0)}$ and $\bar{\phi}^{(0,0)}$ in [38], we obtain

$$\begin{aligned}\bar{J}_1^{(0,0)} =& L_1-R_1-\frac{\alpha\beta(n_1+n_2)(L_1+R_1)}{2(\alpha+\beta)}\\ &+\frac{-\alpha m\bar{V}+\frac{\alpha(\beta n_2-\alpha n_1)}{\alpha+\beta}\left(\frac{(L_1-R_1)s_1-L_1}{s_2-s_1}\ln\left|\frac{1-s_1}{s_1}\right|+\frac{(R_1-L_1)s_2+L_1}{s_2-s_1}\ln\left|\frac{1-s_2}{s_2}\right|\right)}{\left(\frac{1}{s_1-s_2}\ln\left|\frac{1-s_1}{s_1}\right|+\frac{1}{s_2-s_1}\ln\left|\frac{1-s_2}{s_2}\right|\right)},\end{aligned}$$

$$\begin{aligned}\bar{J}_2^{(0,0)} =& L_2-R_2-\frac{\alpha^2(n_1+n_2)(L_1+R_1)}{2(\alpha+\beta)}\\ &+\frac{-\alpha m\bar{V}+\frac{\alpha(\beta n_2-\alpha n_1)}{\alpha+\beta}\left(\frac{(L_1-R_1)s_1-L_1}{s_2-s_1}\ln\left|\frac{1-s_1}{s_1}\right|+\frac{(R_1-L_1)s_2+L_1}{s_2-s_1}\ln\left|\frac{1-s_2}{s_2}\right|\right)}{\left(\frac{1}{s_1-s_2}\ln\left|\frac{1-s_1}{s_1}\right|+\frac{1}{s_2-s_1}\ln\left|\frac{1-s_2}{s_2}\right|\right)},\end{aligned}$$

and

$$\begin{aligned}\bar{\phi}^{(0,0)}(x) =& \bar{V}-\frac{\beta J_2-\alpha J_1}{m(\alpha+\beta)}\left(\frac{1}{s_1-s_2}\ln\left|\frac{x-s_1}{s_1}\right|+\frac{1}{s_2-s_1}\ln\left|\frac{x-s_2}{s_2}\right|\right)\\ &-\frac{\alpha(\beta n_2-\alpha n_1)\left(\frac{\alpha((L_1-R_1)s_1-L_1)\ln\left|\frac{x-s_1}{s_1}\right|}{s_2-s_1}+\frac{\alpha((R_1-L_1)s_2+L_1)\ln\left|\frac{x-s_2}{s_2}\right|}{s_2-s_1}\right)}{m(\alpha+\beta)}.\end{aligned}$$

Here

$$s_1=\frac{m-\alpha(L_1-R_1)+\sqrt{(m-\alpha(L_1-R_1))^2+4mL_1}}{2m}$$

and

$$s_2=\frac{m-\alpha(L_1-R_1)-\sqrt{(m-\alpha(L_1-R_1))^2+4mL_1}}{2m}$$

are two roots of the equation $\alpha(L_1-(L_1-R_1)s)+ms(1-s)=0$.

At our first fixed point iteration, we take a uniform mesh partition as initial mesh and evaluate the functions $(\phi^{(0,0)}, u^{(0,0)}, c_1^{(0,0)}, c_2^{(0,0)}, \bar{J}_1^{(0,0)}, \bar{J}_2^{(0,0)})$ at these mesh points as initial guess for "bvp4c". We use the mesh and solution from previous fixed point iteration as our initial mesh and initial guess for late iteration.

4. An algorithm for numerical detections of V_c and V^c. In this section, we will describe our numerical methods for conducting *Task 2*. For the relatively simple setting in [38], explicit approximation formulas for two critical voltages V_c and V^c are obtained analytically. For general situations, no relevant analytical result is available at this moment. *To be able to take the advantage of numerical I-V curves obtained in Task 1, one needs to design an algorithm that allows numerical detections of these two critical voltages.* Our algorithm relies on *analytical characterizations* of two critical potentials V_c and V^c based on their *defining properties.*

Since we focus on the *ion size effect* on I-V relations, we will treat the radii $r = r_1$ and r_2 (hence $\lambda = r_2/r_1$) as variable parameters, and view L_j's, R_j's, $\varepsilon > 0$ small and a piece-wise constant $Q(x)$ as fixed parameters. Thus, we denote the I-V relation by $I = I(V; \lambda, r)$. For I-V relation corresponding to the classical PNP (ignoring the size effects), we denote it by $I = I_0(V)$.

Definition 4.1. *A solution V_c of*

$$I(V; \lambda, r) = I_0(V), \tag{4.1}$$

will be called a size balance potential. *A solution V^c of*

$$I_\lambda(V; \lambda, r) := \frac{\partial I}{\partial \lambda}(V; \lambda, r) = 0. \tag{4.2}$$

will be called a relative size effect potential.

For fixed (λ, r), the potential V_c will depend on the boundary concentrations L_i's, R_i's and the permanent charge Q. It is the balance potential under which ion sizes do not have effects on the current. The potential V^c is meant to distinguish the magnitudes of effects among different relative ion sizes λ.

Corollary 4.2. *For fixed $(\bar\lambda, \bar r)$, let $\bar V_c$ be a size balance potential defined by (4.1).*

(i) If $I_V(\bar V_c; \bar\lambda, \bar r) > I_{0V}(V_c)$, then $I(V; \lambda, r) > I_0(V)$ for $V > \bar V_c$ but close (that is, the ion sizes enhance the current) and $I(V; \lambda, r) < I_0(V)$ for $V < \bar V_c$ but close (that is, the ion sizes reduce the current).

(ii) If $I_V(\bar V_c; \bar\lambda, \bar r) < I_{0V}(V_c)$, then $I(V; \lambda, r) > I_0(V)$ for $V < \bar V_c$ but close (that is, the ion sizes enhance the current) and $I(V; \lambda, r) < I_0(V)$ for $V > \bar V_c$ but close (that is, the ion sizes reduce the current).

Proof. The proof is simple and we omit it here. □

Remark 4.3. *For the setting considered in ([38]), it was shown ([38, Lemma 6.2]) that $I_V(V; \lambda, r) > I_{0V}(V)$ in (i) holds for all (V, λ) if $r > 0$ is small enough.*

Corollary 4.4. *For fixed (λ_*, r_*), let V_*^c be a potential defined in (4.2). Suppose $I_{\lambda V}(V_*^c; \lambda_*, r_*) \neq 0$. One has, for (V, λ) in a neighborhood of (V_*^c, λ_*),*

(i) if $I_{\lambda V}(V_*^c; \lambda_*, r_*) > 0$, then, for $V > V_*^c$, $I(V; \lambda, r_*)$ is increasing in λ and, for $V < V_*^c$, $I(V; \lambda, r_*)$ is decreasing in λ;

(ii) if $I_{\lambda V}(V_*^c; \lambda_*, r_*) < 0$, then, for $V > V_*^c$, $I(V; \lambda, r_*)$ is increasing in λ and, for $V < V_*^c$, $I(V; \lambda, r_*)$ is decreasing in λ.

Proof. We write, some function $p(V, \lambda)$,

$$I(V; \lambda, r_*) - I(V; \lambda_*, r_*) = p(V, \lambda)(\lambda - \lambda_*).$$

Differentiate with respect to λ and V, and set $\lambda = \lambda_*$ to get

$$I_\lambda(V; \lambda_*, r_*) = p(V, \lambda_*), \quad I_{\lambda V}(V; \lambda_*, r_*) = p_V(V, \lambda_*).$$

In particular, $p(V_*^c, \lambda_*) = 0$ and $p_V(V_*^c, \lambda_*) \neq 0$. It follows from the Implicit Function Theory that there is a function $\Gamma(\lambda)$ for λ near λ_* such that $V_*^c = \Gamma(\lambda_*)$ and $p(\Gamma(\lambda), \lambda) = 0$. Therefore, $p(V, \lambda) = q(V, \lambda)(V - \Gamma(\lambda))$ for some function $q(V, \lambda)$, and

$$q(V_*^c, \lambda_*) = p_V(V_*^c, \lambda_*) = I_{\lambda V}(V_*^c; \lambda_*, r_*).$$

We conclude

$$I_\lambda(V; \lambda_*, r_*) = p(V, \lambda_*) = q(V; \lambda_*)(V - V_*^c).$$

In particular, $I_\lambda(V; \lambda, r_*)$ and $I_{\lambda V}(V_*^c; \lambda_*, r_*)(V - V_*^c)$ have the same sign for (V, λ) in a neighborhood of (V_*^c, λ_*). Both (i) and (ii) then follow immediately. □

Remark 4.5. *For the setting considered in ([38]), it was shown ([38, Lemma 6.2]) that the condition* $I_{\lambda V}(V;\lambda,r)>0$ *in (i) holds for all* (V,λ) *if* $r>0$ *is small enough.*

Given (λ,r), to numerically detect the corresponding critical value(s) V_c, one can simply plot the difference $I(V;\lambda,r)-I_0(V)$ and search for the roots.

Our procedure for a direct numerical detecting of the critical value(s) V^c is based on the following analytical result. For fixed (λ_*,r_*), define

$$H(V,\lambda)=I(V;\lambda,r_*)-I(V;\lambda_*,r_*). \tag{4.3}$$

Proposition 4.6. *For fixed* $(\lambda,r)=(\lambda_*,r_*)$, V_*^c *is the value defined in (4.2) if and only if the point* (V_*^c,λ_*) *is a saddle point of* $H(V,\lambda)$ *under the condition that* $H_{\lambda V}(V_*^c,\lambda_*)=I_{\lambda V}(V_*^c;\lambda_*,r_*)\neq 0$.

Proof. Note that $H(V,\lambda_*)=0$ for all V. Thus, $H_V(V,\lambda_*)=H_{VV}(V,\lambda_*)=0$. From the definition of V_*^c, one has $H_\lambda(V_*^c,\lambda_*)=I_\lambda(V_*^c;\lambda_*,r_*)=0$. Therefore, (V_*^c,λ_*) is a critical point of $H(V,\lambda)$. It then follows from

$$\left(H_{VV}H_{\lambda\lambda}-H_{\lambda V}^2\right)(V_*^c,\lambda_*)=-H_{\lambda V}^2(V_*^c,\lambda_*)<0$$

that (V_*^c,λ_*) is a saddle point of $H(V,\lambda)$. □

Numerically, for fixed (λ_*,r_*), we can computer $I(V;\lambda,r_*)$ and hence $H(V,\lambda)$ for any λ near λ_* and apply Proposition 4.6 to estimate V_*^c from the saddle point of $H(V,\lambda)$. Another approach for detecting V^c is to numerically compute the solution(s) V of $I_\lambda(V;\lambda,r)=0$. This will involve a numerical evaluation of the partial derivative and a numerical root finding.

We remark that, for real biological situations, one is interested in only discrete values of (λ,r). For the critical potential V_c, one can take an experimental I-V relation as $I(V;\lambda,r)$ and numerically (or analytically) compute $I_0(V)$ for ideal case that allows one to get an estimate of V_c. On the other hand, it is not clear to us how to design a procedure of using experimental data to detect the value V^c.

5. Numerical experiments on problem (3.2)–(3.3): case studies.

In this section, we perform numerical simulations to problem (3.2)–(3.3) for different values of α, β, and λ for $Q=0$ and $Q\neq 0$. For simplicity, we will use the following values for the parameters involved in dimensionless PNP-DFT model (3.2)–(3.3):

$$e=1,\ k=1,\ T=1,\ \varepsilon=0.002,\ r_1=r=0.0001.$$

The choice of the numerical values for ε and r as well as the boundary concentrations below are not made from physical considerations although they are in a reasonable range for some physical settings of biological problem. As mentioned above, the main purpose of this case studies is to demonstrate the application of our procedure for finding V_c and V^c directly from numerical I-V relations. As the analysis suggests that the smaller the r value the better the convergence of the fixed point iterations, we test our algorithm with different values of r. To reduce the L_2-error to 10^{-6}, we need 4 fixed point iterations with $r=0.0001$ and 20 iterations with $r=0.001$ for $Q=0$. For the case that $Q(x)=1$ for $x\in(1/3,2/3)$ and $Q(x)=0$ otherwise, to obtain the same accuracy, we need 4 fixed point iterations with $r=0.0001$ and 10 iterations with $r=0.001$. (We observe that the number of iterations for the case with nonzero Q is smaller than or equal to that for $Q=0$. It is surprise to us but does not contradict to our theory.) In the sequel, we only report the results with $r=0.0001$.

5.1. Numerical values vs analytical predications for $Q=0$.

For $Q=0$, we compare the numerical values V_c and V^c with those analytical approximations obtained in [38]. We remark that the analytical values of V_c and V^c in [38] are zeroth order in ε and first order in r approximations. For $\epsilon>0$ small and $r>0$ small, the numerical values V_c and V^c should be close to those obtained from the zeroth order approximation given by (2.9).

In our first set of experiments, we compute V_c for the following 6 different choices of parameter values:

- Case 1: $\alpha = \beta = 1$, $\lambda = 1.885$, $L = \alpha L_1 = \beta L_2 = 4$, and $R = \alpha R_1 = \beta R_2 = 20$;
- Case 2: $\alpha = \beta = 1$, $\lambda = 1.382$, $L = \alpha L_1 = \beta L_2 = 4$, and $R = \alpha R_1 = \beta R_2 = 20$;
- Case 3: $\alpha = 2\beta = 2$, $\lambda = 1.885$, $L = \alpha L_1 = \beta L_2 = 4$, and $R = \alpha R_1 = \beta R_2 = 20$;
- Case 4: $\alpha = \beta = 1$, $\lambda = 1.885$, $L = \alpha L_1 = \beta L_2 = 20$, and $R = \alpha R_1 = \beta R_2 = 4$;
- Case 5: $\alpha = \beta = 1$, $\lambda = 1.382$, $L = \alpha L_1 = \beta L_2 = 20$, and $R = \alpha R_1 = \beta R_2 = 4$;
- Case 6: $\alpha = 2\beta = 2$, $\lambda = 1.885$, $L = \alpha L_1 = \beta L_2 = 20$, and $R = \alpha R_1 = \beta R_2 = 4$.

The choice of $\lambda = 1.885$ in Cases 1, 3, 4, and 6 is motivated by the corresponding λ values for $\mathrm{Na^+Cl^-}$ and $\mathrm{Ca^{2+}Cl_2^-}$, and $\lambda = 1.382$ in Cases 2 and 5 for $\mathrm{K^+Cl^-}$.

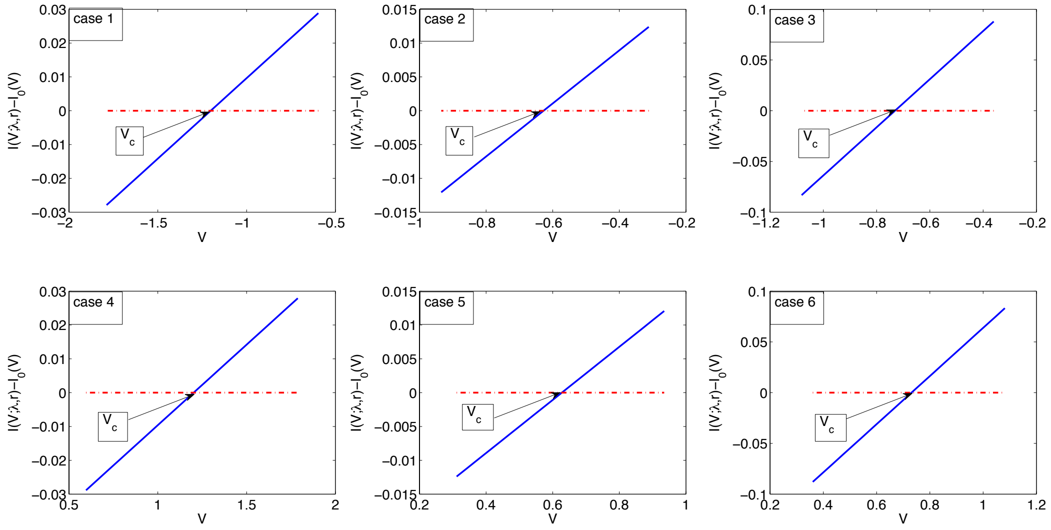

FIG. 5.1. *Plots of $I(V;\lambda,r) - I_0(V)$ and V_c for $Q = 0$.*

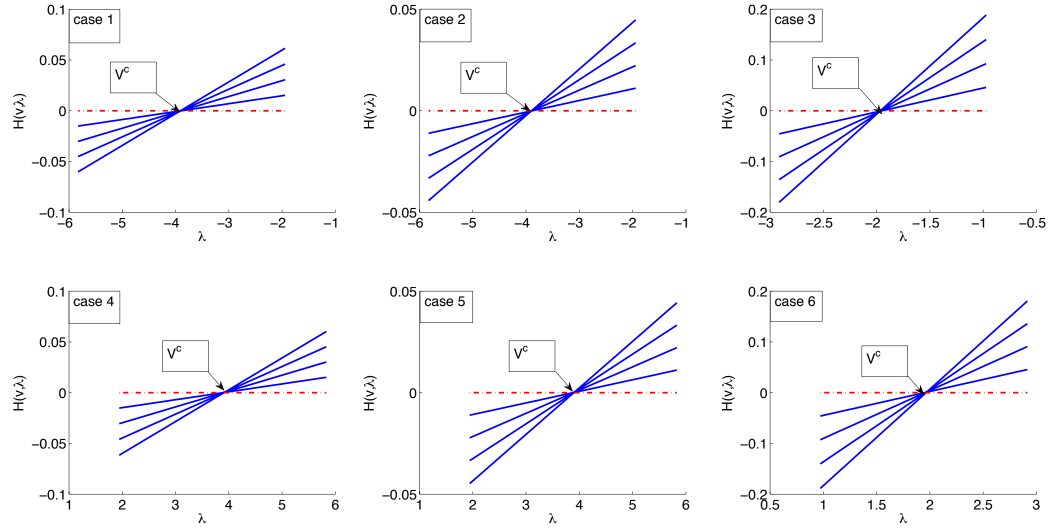

FIG. 5.2. *Plots of $H(V,\lambda)$ with four values of λ and V^c for $Q = 0$.*

For each case, we plot $I(V;\lambda,r) - I_0(V)$ as a function of V and the critical potential V_c is the root of the difference. The results are reported in Figure 5.1. The analytical values of

V_c from (2.9) are -1.1921, -0.6232, and -0.7210 for Cases 1–3, respectively. The numerical values of V_c are -1.2020, -0.6274, and -0.7310, which agree well with the analytical predictions. From the numerical simulations, we observe that V_c's for $L = 4 < R = 20$ (Cases 1–3) and $L = 20 > R = 4$ (Cases 4–6) differ by a sign and the analytical formulas (2.9) for $D_1 = D_2$ verify the observation.

In our second set of experiments, we compute V^c for above 6 cases in the first set of experiments. For each case, we fix $\lambda_* = \lambda/2$ and plot $H(V, \lambda)$, defined in (4.3), as a function of V with 4 different λ values ($3/4\lambda$, λ, $5/4\lambda$, and $6/4\lambda$). The results are in Figure 5.2. The analytical results for zeroth order in ε and first order in r tell us that the graphs for these 4 different λ values should have a common intersection point with $V = V_c$. Also, the analytical values of V^c are -3.8861, -3.8861, and -1.9430 for Cases 1–3, respectively. From Figure 5.2, one sees that these graphs almost go through the same point and the numerical values of V^c are -3.92, -3.92, and -1.96, which are close to the analytical approximations. Similarly, V^c's for $L < R$ and $L > R$ differ by a sign and the analytical formulas (2.9) for $D_1 = D_2$ verify the observation.

5.2. Numerical values of V_c and V^c for piecewise constant $Q(x) \neq 0$. In this section, we consider the problem (3.2)–(3.3) with $Q(x) = Q_0 = 1$ on $(1/3, 2/3)$ and $Q(x) = 0$ otherwise on $[0, 1]$. Due to the jumps of Q, the singularly perturbed auxiliary BVP (3.6)–(3.7) is much **closer to be** singular for small ε. Since we are focusing on the numerical examinations of the critical potentials V_c and V^c, we thus take $\varepsilon = 0.02$ for this study rather than $\varepsilon = 0.002$ as in previous part. Other parameters are the same as the previous section and we will only consider the setting of Case 1.

Applying the strategy described in Section 3.1, we first solve the BVP (3.2)–(3.3) for $V = -0.5960$. The profiles of $\bar{\phi}$ and $\bar{u}$ are shown in Figure 5.3, and those of c_1 and c_2 in Figure 5.4. We observe that $\bar{u}$ have corners around $x = 1/3$ and $x = 2/3$; $c_2 - c_1 \approx Q_0 = 1$ on the interval $(1/3, 2/3)$, where $Q \neq 0$. The presence of the corners of $\bar{u}$ reflects the fact that each transition layer (one at $x = 1/3$ and the other at $x = 2/3$) consists of two portions (see [18, 44]).

The critical potential V_c is determined as we did for $Q = 0$ case and the result is shown in Figure 5.5.

For the critical potential V^c, based on Proposition 4.6, we look for saddle points of $H(V, \lambda)$, whose graph is plotted in Figure 5.6. One clearly sees a saddle point of the surface. The saddle point of this surface will give us the numerical value of V^c.

6. Conclusion. In this paper, motivated by the analytical work in [38], we perform numerical simulations of the one-dimensional version of PNP-DFT system in a general setting to include nonzero but piecewise-constant permanent charges. It is focused on a numerical test and a generalization of the analytical results in [38]. The relatively simple one-dimensional setting of the PNP-DFT system and the analytical approximation of solutions in [38] helps a great deal in our numerical study of the problem. Two numerical tasks are conducted. The first one is a numerical solution of the boundary value problem that allows is to obtain numerical I-V curves. This is accomplished through a numerical implementation of the analytical strategy introduced in [38] for solving the singular boundary value problem of the integro-differential system. We then conducted the second task to numerically detect two critical potential values V_c and V^c. The analytical formulas for V_c and V^c in [38] is clearly only valid for the specific simple setting of the problem in [38]. We thus propose an algorithm based on the defining properties of V_c and V^c and the algorithm allows one to detect these values directly from numerical I-V relations. We also demonstrate the applications of our algorithm in two ways: For the setting in [38] ($Q = 0$ in (3.2)–(3.3)), without using the analytical formulas, the numerical values of V_c and V^c given by the algorithm agree well with the analytical predictions. For a setting including a nonzero permanent charge in (3.2)–(3.3) for which case no analytic formula for the I-V relation is available now, we still can apply the algorithm and find V_c and V^c numerically.

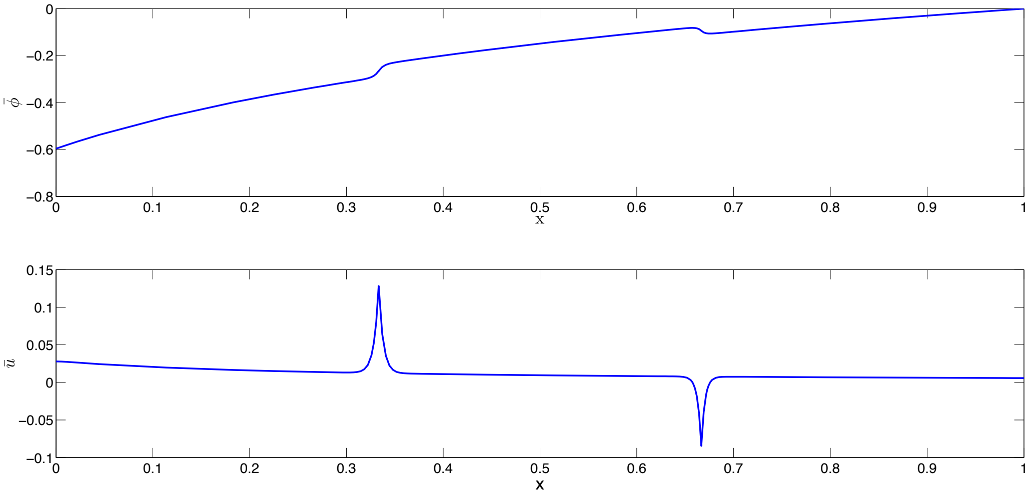

FIG. 5.3. *Profiles of* $\bar{\phi}$ *(top) and* $\bar{u}$ *(bottom) for* $Q \neq 0$.

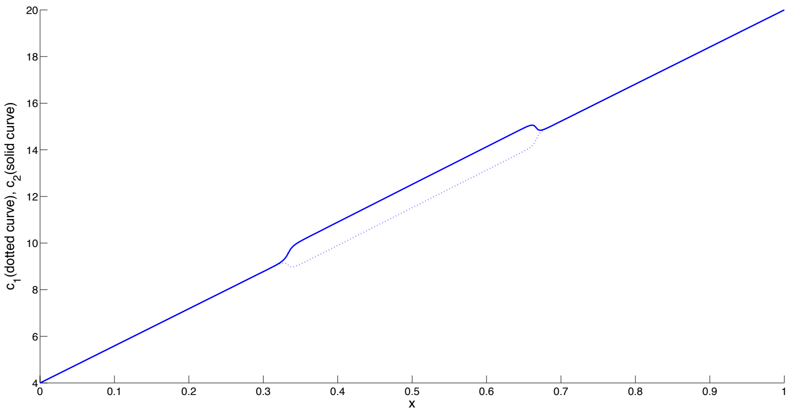

FIG. 5.4. *Profiles of* c_1 *and* c_2 *for* $Q \neq 0$.

It is not expected for the formulas for V_c and V^c in [38] to be applicable directly to realistic settings of biological problems and to general situations. We do believe that the existence of these critical values in general is valid. Needless to say that, for more realistic biological settings involving the three-dimensional geometry of ion channels, all components of excess electrochemical potential, specific choices of dielectric constants and diffusion constants, and biologically meaningful ranges of boundary concentrations, etc., the existence and approximation values of V_c and V^c demand a great deal of investigations, analytically, numerically, and experimentally. We hope our work can stimulate further studies on this and related characteristic values of ion size effects.

REFERENCES

[1] N. Abaid, R. S. Eisenberg, and W. Liu, Asymptotic expansions of I-V relations via a Poisson-Nernst-Planck system. *SIAM J. Appl. Dyn. Syst.* **7** (2008), pp. 1507-1526.

[2] S. Aboud, D. Marreiro, M. Saraniti, and R. S. Eisenberg, A Poisson P3M Force Field Scheme for Particle-Based Simulations of Ionic Liquids. *J. Comput. Electronics* **3** (2004), pp. 117-133.

[3] M. Z. Bazant, M. S. Kilic, B. D. Storey, and A. Ajdari, Towards an understanding of induced-charge

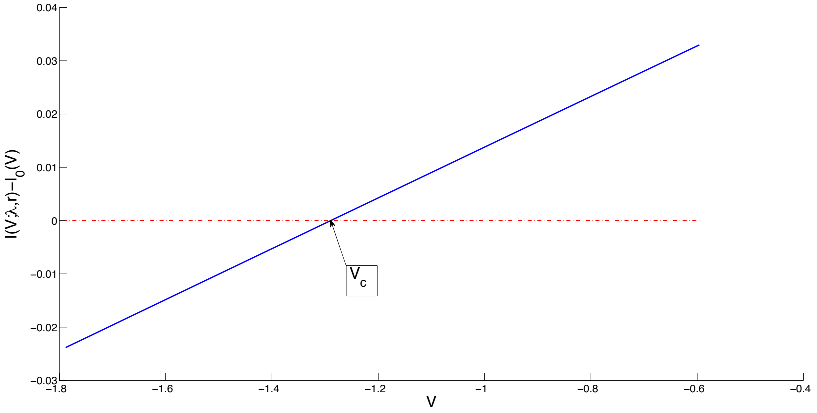

Fig. 5.5. *Plot of $I(V;\lambda,r)-I_0(V)$ and V_c for $Q\neq 0$.*

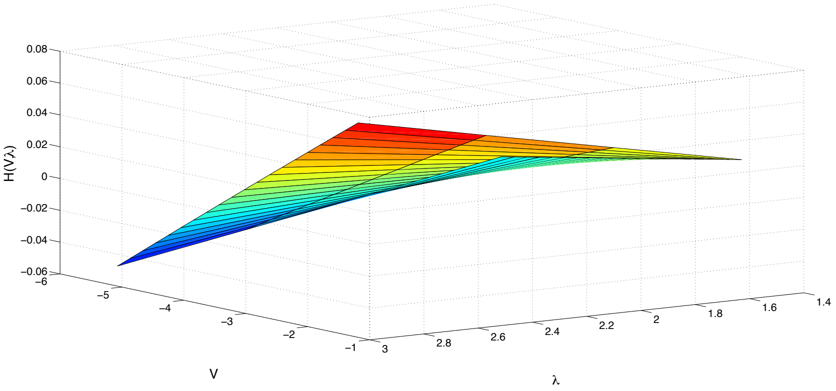

Fig. 5.6. *Plot of $H(V,\lambda)$ whose saddle points give V^c.*

electrokinetics at large applied voltages in concentrated solutions. *Advances in Colloid and Interface Science* **152** (2009), pp. 48-88.

[4] V. Barcilon, Ion flow through narrow membrane channels: Part I. *SIAM J. Appl. Math.* **52** (1992), pp. 1391-1404.

[5] V. Barcilon, D.-P. Chen, and R. S. Eisenberg, Ion flow through narrow membrane channels: Part II. *SIAM J. Appl. Math.* **52** (1992), pp. 1405-1425.

[6] V. Barcilon, D.-P. Chen, R. S. Eisenberg, and J. W. Jerome, Qualitative properties of steady-state Poisson-Nernst-Planck systems: Perturbation and simulation study. *SIAM J. Appl. Math.* **57** (1997), pp. 631-648.

[7] D. Boda, D. Gillespie, W. Nonner, D. Henderson, and B. Eisenberg, Computing induced charges in inhomogeneous dielectric media: application in a Monte Carlo simulation of complex ionic systems. *Phys. Rev. E* **69** (2004), pp. 046702 (1-10).

[8] D. Boda, D. Busath, B. Eisenberg, D. Henderson, and W. Nonner, Monte Carlo simulations of ion selectivity in a biological Na+ channel: charge-space competition. *Phys. Chem. Chem. Phys.* **4** (2002), pp. 5154-5160.

[9] M. Burger, R. S. Eisenberg, and H. W. Engl, Inverse problems related to ion channel selectivity. *SIAM J. Appl. Math.* **67** (2007), pp. 960-989.

[10] A. E. Cardenas, R. D. Coalson, and M. G. Kurnikova, Three-Dimensional Poisson-Nernst-Planck Theory Studies: Influence of Membrane Electrostatics on Gramicidin A Channel Conductance. *Biophys. J.* **79** (2000), pp. 80-93.

[11] D. P. Chen and R.S. Eisenberg, Charges, currents and potentials in ionic channels of one conformation. *Biophys. J.* **64** (1993), pp. 1405-1421.

[12] S. Chung and S. Kuyucak, Predicting channel function from channel structure using Brownian dynamics simulations. *Clin. Exp. Pharmacol Physiol.* **28** (2001), pp. 89-94.

[13] R.D. Coalson, Poisson-Nernst-Planck theory approach to the calculation of current through biological ion channels. *IEEE Trans Nanobioscience* **4** (2005), pp. 81-93.

[14] R.D. Coalson, Discrete-state model of coupled ion permeation and fast gating in ClC chloride channels. *J. Phys. A* **41** (2009), 115001.

[15] R. Coalson and M. Kurnikova, Poisson-Nernst-Planck theory approach to the calculation of current through biological ion channels. *IEEE Transaction on NanoBioscience* **4** (2005), pp. 81-93.

[16] B. Eisenberg, Y. Hyon, and C. Liu, Energy variational analysis of ions in water and channels: Field theory for primitive models of complex ionic fluids. *J. Chem. Phys.* **133** (2010), pp. 104104 (1-23).

[17] B. Eisenberg, Y. Hyon, and C. Liu, Energy variational analysis *EnVarA* of ions in calcium and sodium channels: Field theory for primitive models of complex ionic fluids. *Biophys. J.* **98** (2010), p. 515a.

[18] B. Eisenberg and W. Liu, Poisson-Nernst-Planck systems for ion channels with permanent charges. *SIAM J. Math. Anal.* **38** (2007), pp. 1932-1966.

[19] R. Evans, The nature of the liquid-vapour interface and other topics in the statistical mechanics of non-uniform, classical fluids. *Adv. Phys.* **28** (1979), pp. 143-200.

[20] R. Evans, Density functionals in the theory of nonuniform fluids, in *Fundamentals of of inhomogeneous fluids*, ed. D. Henderson (New York: Dekker), pp. 85-176, (1992).

[21] J. Fischer and U. Heinbuch, Relationship between free energy density functional, Born-Green-Yvon, and potential distribution approaches for inhomogeneous fluids. *J. Chem. Phys.* **88** (1988), pp. 1909-1913.

[22] D. Gillespie, A singular perturbation analysis of the Poisson-Nernst-Planck system: Applications to Ionic Channels. *Ph.D Dissertation*, Rush University at Chicago, 1999.

[23] D. Gillespie, L. Xu, Y. Wang, and G. Meissner, (De)constructing the Ryanodine Receptor: Modeling Ion Permeation and Selectivity of the Calcium Release Channel. *J. Phys. Chem. B* **109** (2005), pp. 15598-15610.

[24] D. Gillespie, Energetics of Divalent Selectivity in a Calcium Channel: The Ryanodine Receptor Case Study. *Biophys. J.* **94** (2008), pp. 1169-1184.

[25] D. Gillespie, Intracellular Calcium Release Channels Mediate Their Own Countercurrent: The Ryanodine Receptor Case Study. *Biophys. J.* **95** (2008), pp. 3706-3714.

[26] D. Gillespie, J. Giri, and M. Fill, Reinterpreting the Anomalous Mole Fraction Effect: The Ryanodine Receptor Case Study *Biophys. J.* **97** (2009), pp. 2212-2221.

[27] D. Gillespie and R. S. Eisenberg, Modified Donnan potentials for ion transport through biological ion channels. *Phys. Rev. E* **63** (2001), pp. 061902 (1-8).

[28] D. Gillespie and R. S. Eisenberg, Physical descriptions of experimental selectivity measurements in ion channels. *European Biophys. J.* **31** (2002), pp. 454-466.

[29] D. Gillespie, W. Nonner, and R. S. Eisenberg, Coupling Poisson-Nernst-Planck and density functional theory to calculate ion flux. *J. Phys.: Condens. Matter* **14** (2002), pp. 12129-12145.

[30] D. Gillespie, W. Nonner, and R.S. Eisenberg, Density functional theory of charged, hard-sphere fluids. *Phys. Rev. E* **68** (2003), pp. 0313503 (1-10).

[31] P. Graf, M.G. Kurnikova, R.D. Coalson, and A. Nitzan, Comparison of Dynamic Lattice Monte-Carlo Simulations and Dielectric Self Energy Poisson-Nernst-Planck Continuum Theory for Model Ion Channels. *J. Phys. Chem. B* **108** (2004), pp. 2006-2015.

[32] U. Hollerbach, D.-P. Chen, and R.S. Eisenberg, Two- and Three-Dimensional Poisson-Nernst-Planck Simulations of Current Flow through Gramicidin-A. *J. Comp. Science* **16** (2002), pp. 373-409.

[33] U. Hollerbach, D. Chen, W. Nonner, and B. Eisenberg, Three-dimensional Poisson-Nernst-Planck Theory of Open Channels. *Biophys. J.* **76** (1999), p. A205.

[34] Y. Hyon, B. Eisenberg, and C. Liu, A mathematical model for the hard sphere repulsion in ionic solutions. *Commun. Math. Sci.* **9** (2010), pp. 459-475.

[35] Y. Hyon, J. Fonseca, B. Eisenberg, and C. Liu, A new Poisson-Nernst-Planck equation (PNP-FS-IF) for charge inversion near walls. *Biophys. J.* **100** (2011), pp. 578a.

[36] W. Im, D. Beglov, and B. Roux, Continuum solvation model: Electrostatic forces from numerical solutions to the Poisson-Bolztmann equation. *Comp. Phys. Comm.* **111** (1998), pp. 59-75.

[37] W. Im and B. Roux, Ion permeation and selectivity of OmpF porin: a theoretical study based on molecular dynamics, Brownian dynamics, and continuum electrodiffusion theory. *J. Mol. Biol.* **322** (2002), pp. 851-869.

[38] S. Ji and W. Liu, Poisson-Nernst-Planck Systems for Ion Flow with Density Functional Theory for Hard-Sphere Potential: I-V relations and critical potentials. Part I: Analysis (submitted).

[39] M.S. Kilic, M.Z. Bazant, and A. Ajdari, Steric effects in the dynamics of electrolytes at large applied voltages. II. Modified Poisson-Nernst-Planck equations. *Phys. Rev. E* **75** (2007), 021503 (11 pages).

[40] J. Kierzenka, and L. Shampine, A BVP Solver Based on Residual Control and the Matlab PSE. *ACM Trans. Math. Software* **27** (2001), pp. 299-316.

[41] M. Knepley, D. karpeev, S. Davidovits, R. eisenberg, D. Gillespie, An efficient algorithm for classical density functional theory in three dimensions: Ionic solutions. *J. Chem. Phys* **132** 124101 (2010).

[42] M. G. Kurnikova, R.D. Coalson, P. Graf, and A. Nitzan, A Lattice Relaxation Algorithm for 3D Poisson-Nernst-Planck Theory with Application to Ion Transport Through the Gramicidin A Channel. *Biophys. J.* **76** (1999), pp. 642-656.

[43] W. Liu, Geometric singular perturbation approach to steady-state Poisson-Nernst-Planck systems. *SIAM J. Appl. Math.* **65** (2005), pp. 754-766.

[44] W. Liu, One-dimensional steady-state Poisson-Nernst-Planck systems for ion channels with multiple ion species. *J. Differential Equations* **246** (2009), pp. 428-451.

[45] M. S. Mock, An example of nonuniqueness of stationary solutions in device models. *COMPEL* **1** (1982),

pp. 165-174.

[46] B. Nadler, U. Hollerbach, and R.S. Eisenberg, Dielectric boundary force and its crucial role in gramicidin. *Phys. Rev. E* **68** (2003), pp. 021905 (1-9).

[47] B. Nadler, Z. Schuss, A. Singer, and B. Eisenberg, Diffusion through protein channels: from molecular description to continuum equations. *Nanotech.* **3** (2003), pp. 439-442.

[48] W. Nonner and R. S. Eisenberg, Ion permeation and glutamate residues linked by Poisson-Nernst-Planck theory in L-type Calcium channels. *Biophys. J.* **75** (1998), pp. 1287-1305.

[49] S.Y. Noskov, W. Im, and B. Roux, Ion Permeation through the α-Hemolysin Channel: Theoretical Studies Based on Brownian Dynamics and Poisson-Nernst-Planck Electrodiffusion Theory. *Biophys. J.* **87** (2004), pp. 2299-2309.

[50] J.-K. Park and J. W. Jerome, Qualitative properties of steady-state Poisson-Nernst-Planck systems: Mathematical study. *SIAM J. Appl. Math.* **57** (1997), pp. 609-630.

[51] J. K. Percus, Equilibrium state of a classical fluid of hard rods in an external field. *J. Stat. Phys.* **15** (1976), pp. 505-511.

[52] J. K. Percus, Model grand potential for a nonuniform classical fluid. *J. Chem. Phys.* **75** (1981), pp. 1316-1319.

[53] A. Robledo and C. Varea, On the relationship between the density functional formalism and the potential distribution theory for nonuniform fluids. *J. Stat. Phys.* **26** (1981), pp. 513-525.

[54] Y. Rosenfeld, Free-Energy Model for the Inhomogeneous Hard-Sphere Fluid Mixture and Density-Functional Theory of Freezing. *Phys. Rev. Lett.* **63** (1989), pp. 980-983.

[55] Y. Rosenfeld, Free energy model for the inhomogeneous fluid mixtures: Yukawa-charged hard spheres, general interactions, and plasmas. *J. Chem. Phys.* **98** (1993), pp. 8126-8148.

[56] B. Roux, T.W. Allen, S. Berneche, and W. Im, Theoretical and computational models of biological ion channels. *Quat. Rev. Biophys.* **37** (2004), pp. 15-103.

[57] B. Roux, Theory of Transport in Ion Channels: From Molecular Dynamics Simulations to Experiments, in *Comp. Simul. In Molecular Biology*, J. Goodefellow ed., VCH Weinheim, Ch. 6, pp. 133-169 (1995).

[58] I. Rubinstein, Multiple steady states in one-dimensional electrodiffusion with local electroneutrality. *SIAM J. Appl. Math.* **47** (1987), pp. 1076-1093.

[59] I. Rubinstein, *Electro-Diffusion of Ions.* SIAM Studies in Applied Mathematics, SIAM, Philadelphia, PA, 1990.

[60] M. Saraniti, S. Aboud, and R. Eisenberg, The Simulation of Ionic Charge Transport in Biological Ion Channels: an Introduction to Numerical Methods. *Rev. Comp. Chem.* **22** (2005), pp. 229-294.

[61] Z. Schuss, B. Nadler, and R. S. Eisenberg, Derivation of Poisson and Nernst-Planck equations in a bath and channel from a molecular model. *Phys. Rev. E* **64** (2001), pp. 1-14.

[62] A. Singer and J. Norbury, A Poisson-Nernst-Planck model for biological ion channels–an asymptotic analysis in a three-dimensional narrow funnel. *SIAM J. Appl. Math.* **70** (2009), pp. 949-968.

[63] A. Singer, D. Gillespie, J. Norbury, and R. S. Eisenberg, Singular perturbation analysis of the steady-state Poisson-Nernst-Planck system: applications to ion channels. *European J. Appl. Math.* **19** (2008), pp. 541-560.

[64] H. Steinrück, Asymptotic analysis of the current-voltage curve of a *pnpn* semiconductor device. *IMA J. Appl. Math.* **43** (1989), pp. 243–259.

[65] H. Steinrück, A bifurcation analysis of the one-dimensional steady-state semiconductor device equations. *SIAM J. Appl. Math.* **49** (1989), pp. 1102–1121.

[66] T. A. van der Straaten, G. Kathawala, R.S. Eisenberg, and U. Ravaioli, BioMOCA - a Boltzmann transport Monte Carlo model for ion channel simulation. *Molecular Simul.* **31** (2004), pp. 151-171.